PHYSICAL REVIEW B **69**, 020106(R) (2004)

Dynamic simulation of pressure-driven phase transformations in crystalline Al_2O_3

Sandro Jahn and Paul A. Madden
Physical and Theoretical Chemistry Laboratory, Oxford University, South Parks Road, Oxford OX1 3QZ, United Kingdom

Mark Wilson
Department of Chemistry, University College London, 20 Gordon Street, London WC1H 0AJ, United Kingdom
(Received 2 September 2003; published 27 January 2004)

The pressure-driven phase behavior of crystalline Al_2O_3 is studied using molecular dynamics with an interaction model derived directly from *ab initio* calculations. The application and removal of pressure results in two phase transformations to and from the Rh_2O_3-II and, at higher pressure, an orthoperovskite phase, respectively. The x-ray diffraction pattern of the orthoperovskite phase is compatible with the experimental data and its stability can be rationalized in terms of changes in the ion coordination environments and corundum grain boundaries. Implications for pressure measurements using Ruby fluorescence lines are discussed.

DOI: 10.1103/PhysRevB.69.020106 PACS number(s): 64.70.−p, 61.72.Mm, 62.50.+p

Crystalline alumina Al_2O_3 doped with Cr^{3+} (Ruby), is widely used as a pressure marker in high-pressure experiments.[1] The fluorescence lines show a clear pressure dependence which allows for the monitoring of the *in situ* pressure in a sample held in a diamond anvil cell. However, as the pressures accessed in such experiments increase, a detailed atomistic understanding of the behavior of this marker becomes important as potential phase transitions may alter the fluorescence properties.

Alumina, in common with a range of M_2O_3 stoichiometry oxides, crystallizes under ambient conditions into a corundum ($\alpha-Al_2O_3$) structure in which all the cations are in a six-coordinate environment. Under pressure, such systems may transform into a Rh_2O_3-II structure (in which the cations are also six-coordinate) (Ref. 2) as has been observed for Cr_2O_3,[3] Fe_2O_3 (Refs. 4,5) and Rh_2O_3 itself.[2] For Al_2O_3, the Rh_2O_3-II structure has been reported from x-ray diffraction experiments to appear at $\sim$100 GPa.[6] In addition, the results of electronic structure calculations[7] have been used to argue that such a structure has been seen previously at $\sim$175 GPa.[8] The experimental evidence for the appearance of this structure is, however, not entirely compelling. The high pressures and temperatures, coupled with diffraction peaks arising from impurities, necessary containment materials, and possible residual corundum material, render the experimental diffraction patterns open to alternative interpretations.

Ab initio electronic structure techniques have been utilized in order to locate the pressure at which the corundum to Rh_2O_3-II (as well as other possible high-pressure structures based on a distorted perovskite) phase transition becomes thermodynamically favored.[7,9] These methodologies do not, however, lend themselves naturally to the study of dynamic pressure-driven transitions which may lead to information regarding the transformation kinetics. The computational expense of even the most efficient methodologies severely restricts both the length and time scales which can be effectively studied. By referring to a simpler representation of the ion properties a more computationally efficient model can be constructed that allows for the study of the time-dependent dynamics and, as a result, may lead to an understanding of the atomistic mechanisms by which such phase transformations occur. Furthermore, the use of a truly dynamic approach may allow for the evolution of structures previously unimagined, or distortions of structures already considered, which may then act as a symbiotic feed into additional well-directed electronic structure calculations.

In order to account for the relative sensitivity of the oxide anion to the ion environment a flexible representation of the response of the ion electron density to changes in that environment is required. This model, termed an anisotropic-ion model (AIM),[10,11] incorporates the response of each ion to changes in the electric field and gradient (induced dipoles and quadrupoles) and their deformation (change in both size and shape) in response to changes in the local (short-range) environment. The parameters required for the AIM are obtained by utilizing force-fitting procedures.[11] Reference density-functional calculations are performed on five different atomic configurations taken from molecular dynamics simulations on systems containing around 200 ions. These configurations are taken from different crystal structures and the liquid state and hence a range of possible coordination environments are sampled in the fitting. Each configuration yields a set of *ab initio* individual ion forces, $\{f_\alpha^i\}$, and cell stress tensors, $\{\eta_{ab}\}$. The Kohn-Sham orbitals are subjected to a Wannier analysis which allows the inherent ion dipoles and quadrupoles, $\{\mu_\alpha^i, \theta_{\alpha\beta}^i\}$, to be extracted from each configuration.[12] Up to 21 of the AIM parameters are then varied in several steps within physically reasonable limits in order to best fit the complete set of forces, stresses and ion multipoles, $\{f_\alpha^i, \eta_{ab}, \mu_\alpha^i, \theta_{\alpha\beta}^i\}$.

Figure 1 shows the static (0 K) energy/volume curves for the Al_2O_3 AIM calculated for the corundum, Rh_2O_3-II and the orthorhombic-distorted perovskite (see Ref. 7) structures. The ion coordinates and cell variables are relaxed at each volume. The pressure at which the Rh_2O_3-II structure becomes thermodynamically stable over the corundum can be calculated by equating the respective free energies (simply given by $U+pV$ for each phase at 0 K, with $p=-dU/dV$). The present model predicts a transition pressure of 90 GPa consistent with the most recent electronic structure value [78 GPa (Ref. 7) which compares with older values between 6 and 148 GPa (Refs. 13–16)] and the experi-

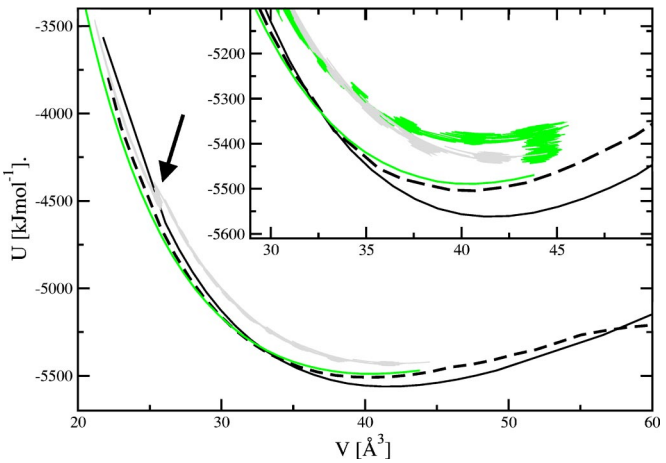

FIG. 1. (Color online) Energy/volume curves for the corundum (solid line), Rh_2O_3-II (dashed line) and orthoperovskite (light line) structures. The lightest line shows the dynamic evolution of the energy for the corundum $\rightarrow Rh_2O_3$-II$\rightarrow$ orthoperovskite transformation. The arrow indicates the location of the two-stage transformation. The inset shows the region around the respective energy minima in more detail with the addition of a (light) curve showing the dynamic evolution of the energy for the reverse (Rh_2O_3-II$\rightarrow$ corundum) transformation.

mental value of $\sim$100 GPa.[6] The present model value is significantly less than the value of 194 GPa predicted using a less sophisticated version of the current model in which only the change in size (and not shape) of the anion was considered.[17] The volume change is predicted to be $\sim$2.1% compared with $\sim$2.2% (Ref. 7) and $\sim$1.7–2.5%.[13–17] The experimental volume change is estimated to be $\sim$3.7%.[6]

Dynamic simulations are performed starting from the corundum structure with 32 Al_2O_3 units. The variables controlling the AIM are incorporated as variational degrees of freedom in an extended Lagrangian formalism and the energy minimized with respect to them using a conjugate gradient algorithm.[18] The system temperature is maintained at 1000 K using Nosé-Hoover thermostats[19] with the pressure controlled by anisotropic barostats, in which the cell lengths and angles are allowed to vary in order to maintain a constant stress.[20] A molecular dynamics time-step of 50 a.u. ($\sim$1.2 fs) is employed and changes in the pressure are imposed by incrementing the required barostat pressure in steps of 0.0002 a.u. ($\cong$5.9 GPa) every 4000 steps ($\cong$5 ps). Analysis of the changes in the system cell lengths, angles, volume, and the total structure factors as a function of time indicate that two structural transformations occur up to a pressure of around 270 GPa with no further changes in cell angles observed up to 500 GPa. The two changes occur in close succession are $\sim$270 and 278 GPa with associated volume changes of $\sim$2.7% and 0.4%, respectively. These large overpressures are discussed below. The dynamic evolution of the system energy as a function of the volume as the pressure is increased is shown in Fig. 1 superimposed on the static (0 K) energy/volume curves. The phase transitions are clearly evident as a sharp change in the energy and volume (highlighted by the arrow).

Figure 2 shows the total x-ray scattering functions $F^{xrd}(k)$ calculated by combining the three partial structure factors, $S_{\alpha\beta}(k)=\langle A_\alpha(k).A^*_\beta(k)\rangle$, where $A_\alpha(k)=(1/\sqrt{N_\alpha})\Sigma_{i=1}^{N_\alpha}e^{ik.r_i}$, weighted by the appropriate form factors.[21] The figure shows this function calculated dynamically by averaging over 100 configurations ($\cong$12 ps) and that generated from the inherent structures (the nearest local potential energy minima found from these configurations). Three distinct diffraction patterns are evident as the pressure-driven transition evolves. Prior to the first volume change the diffraction pattern clearly resembles that for corundum (as evidenced by the peak assignments shown). After the first (largest) volume change the diffraction pattern corresponds to that expected for the Rh_2O_3-II structure with, in particular, the emergence of the [011] peak. The highest pressure structure observed in the present work (present after the second, smaller, volume change) yields the uppermost diffraction pattern. The diffraction pattern is similar to those observed for both the corundum and Rh_2O_3-II structures, with additional peaks evident at low scattering angle ($\sim$1.9 Å^{-1}) and $\sim$3.2 Å^{-1}. Further analysis shows the latter to correspond to an orthoperovskite structure.

Figure 2 also shows molecular graphics ''snapshots'' of the three inherent structures, projected along the $[\bar{1}2\bar{1}0]$ direction. The bottom and center snapshots correspond to the corundum and Rh_2O_3-II structures, respectively. Both crystal structures are constructed exclusively from six-coordinate cations and four-coordinate anions. The Rh_2O_3-II structure can be considered as constructed from slices of the corundum structure[2] giving an infinite series of vacancy-terminated $\{\bar{1}012\}\|\{\bar{1}012\}$ rhombohedral twin grain boundaries, in which successive slabs are related to one another by a screw rotation about the $[10\bar{1}1]$ direction.[22] As a result, the pressure-driven transition from the corundum $\rightarrow Rh_2O_3$-II structures appears relatively unusual in that there is no increase in the nominal nearest-neighbor cation-anion coordination number. However, the transformation does allow for a relaxation of the mean Al-O bond length as one of the three ''short'' Al-O bonds in the corundum structure is transformed to a ''long'' bond in the Rh_2O_3-II. As a result, there is an increase of around 2.5% in the mean Al-O bond length (calculated for the first six anion neighbors) across the phase transformation.

The uppermost snapshot in Fig. 2 shows the orthoperovskite structure found to be stable in the present model up to $\sim$500 GPa. At these high pressures the perovskite structure formed is found to be a distortion of that considered previously.[7] The oxygen atom (labeled $O^{(1)}$ in Ref. 7) is displaced from (0.142,0.412,0.250) in the original unit cell, to (0.941,0.342,0.250). The ions labeled $O^{(2)}$ and $Al^{(2)}$ show small displacements. As a result of this distortion, this structure can also be rationalized as a series of $\{\bar{1}012\}\|\{\bar{1}012\}$ grain boundaries but which are now effectively anion terminated.[22] However, unlike the Rh_2O_3-II structure, the formation of this grain boundary sequence does lead to a change in the cation-anion coordination environment. The 50% of the cations which occupy the sites along each boundary are in effective eight-coordinate (six short and two longer bonds) sites. As a result, the stability of this high pressure structure can be understood in terms of the increase in cation-anion coordination number. To emphasize this point, Fig. 1 shows the 0 K energy/volume curve for the idealized

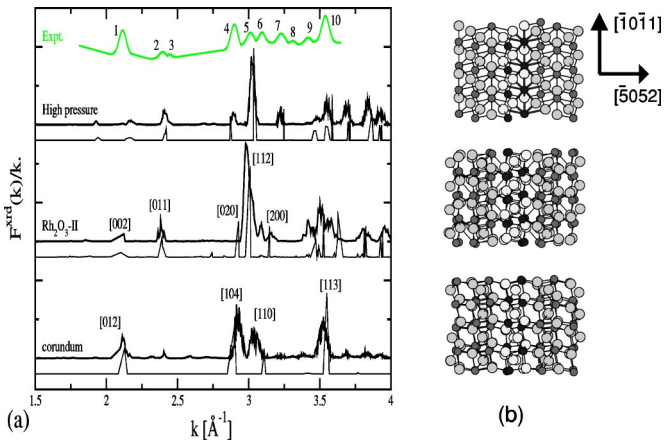

FIG. 2. (Color online) (a) Total x-ray diffraction pattern [shown as $F^{xrd}(k)/k$ to emphasize the low-k features] for the corundum, Rh_2O_3-II and high-pressure grain boundary (orthoperovskite) structures. The upper (thick) lines are time-averaged over 100 configurations while the lower (thin) lines are calculated from single (inherent structure) configurations. The uppermost curve is the experimental high pressure ($\sim$100 GPa) from Ref. 6. (b) Molecular graphics ''snapshots'' of the three inherent structures taken during the dynamic phase transformations projected along the [$\bar{1}2\bar{1}0$] direction. The top figure (the orthoperovskite) is viewed in a direction equivalent to the [110] direction in the orthoperovskite unit cell.

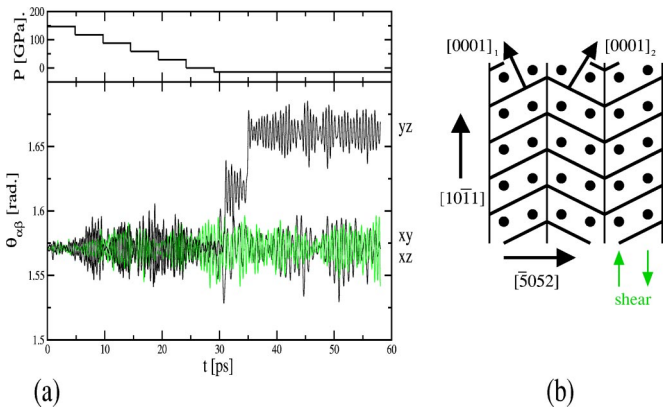

FIG. 3. (Color online) (a) Time evolution of the three cell angles for the Rh_2O_3-II$\rightarrow$ corundum transformation. The systematic two-step change in θ_{yz} is indicative of successive $\{\bar{1}012\}\|\{\bar{1}012\}$ grain boundary annihilations. (b) Schematic representation of the observed Rh_2O_3-II$\rightarrow$ corundum shearing mechanism. The thick black lines represent layers of anions on the {0001} planes of each grain. The solid circles represent the locations of the cations between these anion planes. The shearing motion indicated by the arrows transforms the anion planes into a single sequence of (corundum) stacked {0001} planes.

orthoperovskite structure. As expected, the higher mean anion-cation coordination number structure becomes energetically stable at low volumes. Additional high-pressure electronic structure calculations, in which the cell and ion coordinates are allowed to fully relax, confirm the stability of this orthoperovskite structure. Furthermore, these calculations confirm the relative energetic stabilities of the corundum, Rh_2O_3-II and orthoperovskite structures.

Figure 2 shows the experimental high pressure ($\sim$100 GPa) x-ray diffraction pattern determined by Funamori and Jeanloz.[6] The relatively facile formation of the orthoperovskite structure, and its clear relationship to the Rh_2O_3-II, allows us to speculate that this, and not the Rh_2O_3-II structure, may be giving rise to the experimentally observed x-ray diffraction pattern.[6] To aid the interpretation of the experimental XRD pattern shown in Fig. 2, the first ten peaks have been labeled. Peaks 1 and 2 appear in both the high pressure and Rh_2O_3-II patterns. The peak at low scattering angle (at $\sim$1.9 Å^{-1}) in the orthoperovskite structure is not evident in the experimental pattern, although it may be hidden by the increase in signal observed at such low scattering angles. Peak 4 does not appear in the pattern derived from the Rh_2O_3-II structure, but is evident from the orthoperovskite structure. Funamori and Jeanloz reasonably argue that their experimental high-pressure sample may contain a mixture of the high-pressure structure and the corundum (low pressure) starting material. As a result, peak 4 is argued to arise from the [104] corundum peak. An analogous argument is used to explain the absence of peak 7 in the Rh_2O_3-II derived x-ray diffraction pattern (which is present in the high-pressure pattern). In this case, the presence of the Pt gasket material in the sample is cited as the peak origin.

In summary, therefore, the high-pressure grain boundary structure (equivalent to an orthoperovskite crystal) observed in the present work is, at least, as good a fit to the experimentally determined high pressure x-ray diffraction pattern as is the Rh_2O_3-II-derived pattern. An improvement in the quality of the x-ray diffraction patterns or, alternatively, a neutron study (which would lead to a very different scattering pattern owing to the different ion scattering properties) could lead to a more accurate interpretation of the underlying structures. Alternatively, ^{27}Al NMR techniques would show a different chemical shift for the two aluminum environments (see, for example, Ref. 23). However, present techniques do not allow for such samples to be studied at high pressures.

To further understand the transformation mechanism dynamic simulations are performed in which the pressure is systematically decreased from the maximum value reached (500 GPa) to ~ -15 GPa in steps of -0.0002 a.u. every 4000 steps. As with the positive pressure-gradient process, two transformations are observed by reference to the cell volumes, angles and lengths, at $\sim$150 GPa and ~ -15 GPa, respectively, with associated volume changes of 0.9% and 2.2%, respectively. Analysis of the x-ray diffraction patterns shows that these two transformations are the reverse of those observed for the positive pressure cycle; the transformation at $\sim$150 GPa corresponds to the orthoperovskite $\rightarrow Rh_2O_3$-II, while that at ~ -15 GPa corresponds to the Rh_2O_3-II$\rightarrow$ corundum.

Figure 3(a) shows the time-evolution of the three cell angles for the second transformation (Rh_2O_3-II$\rightarrow$ corundum). The evolution of the required system pressure as a function of time is shown in the upper panel. The cell undergoes a clear two-step change in shape from orthorhombic to monoclinic with the angle between the b and c axes, θ_{bc}, changing from 90° to $\sim$95°. An analysis of the ion positions indicates that the distinct two-step process indicated by Fig.

3(a) are the result of the annihilation of successive vacancy-terminated $\{\bar{1}012\}\|\{\bar{1}012\}$ grain boundaries. The evolution of the dynamic system energy, as a function of volume, is shown in the inset to Fig. 1 with the phase transformation back to the corundum indicated by the change in system energy. Figure 3(b) shows a schematic representation of the mechanism by which the Rh_2O_3-II structure transforms into the corundum. The grains in the Rh_2O_3-II structure have alternately arranged close-packed anion sublattices (as indicated by the $[0001]_1$ and $[0001]_2$ directions in the figure). The transformation to the corundum structure requires these lattices to revert to a single close-packed anion sublattice direction. This is achieved by a shearing motion in which the anions on the grain boundary edges are seen to translate along opposite directions. As a result, one of the $[0001]$ directions in the Rh_2O_3-II crystal reverts to the alternate $[0001]$ direction with an effective rotation in the sub-lattice of 74.3°.

The highly correlated ion motion required for the corundum $\leftrightarrow Rh_2O_3$-II transformations indicates that such a structural change should have a high kinetic barrier. Furthermore, the symmetry breaking required for the corundum $\rightarrow Rh_2O_3$-II transformation may introduce a further kinetic barrier. These barriers are evident in the large over- and under-pressures required to drive the transformations in the simulation model. The addition symmetry-breaking element is manifested in the larger over pressure observed when compared with the under pressure. The Rh_2O_3-II$\leftrightarrow$ orthoperovskite transformation is, however, relatively facile as it involves a systematic shift of the corundumlike grains evident in Fig. 2(b).

Finally, the relatively facile formation of the high-pressure grain boundary structure (orthoperovskite) observed here may have significant implications for the Cr^{3+}-doped Ruby pressure markers. The Cr^{3+} ion, being larger than the Al^{3+}, would be expected to segregate to the larger eight-coordinate sites (in a manner highlighted by Elsässer and Marinopoulos[24] for doped alumina). Such segregation may control the frequencies of the fluorescence lines at extreme pressures.

M.W. thanks the Royal Society for financial support. The work was supported by EPSRC grants (Grants Nos. GR/S06233/01 and GR/R57584/01).

[1] R.J. Nelmes, and M.I. McMahon, Semicond. Semimetals **54**, 145 (1998).
[2] A. F. Wells, *Structural Inorganic Chemistry* (Clarendon, Oxford, 1984).
[3] J. Mougin, T. Le Bihan, and G. Lucazeau, J. Phys. Chem. Solids **62**, 553 (2001).
[4] G.Kh. Rozenberg, L.S. Dubrovinsky, M.P. Pasternak, O. Naaman, T. Le Bihan, and R. Ahuja, Phys. Rev. B **65**, 064112 (2002).
[5] M.P. Pasternak, G.Kh. Rozenberg, G.Yu. Machavariani, O. Naaman, R.D. Taylor, and R. Jeanloz, Phys. Rev. Lett. **82**, 4663 (1999).
[6] N. Funamori and R. Jeanloz, Science **278**, 1109 (1997).
[7] K.T. Thomson, R.M. Wentzcovitch, and M.S.T. Bukowinski, Science **274**, 1880 (1996); W. Duan, G. Paiva, R.M. Wentzcovitch, and A. Fazzio, Phys. Rev. Lett. **81**, 3267 (1998); W. Duan, R.M. Wentzcovitch, and K.T. Thomson, Phys. Rev. B **57**, 10 363 (1998).
[8] A.P. Jephcoat, R.J. Hemley, H.K. Mao, and K.A. Goettel, Physica B **B150**, 116 (1988).
[9] R. Franco, J.M. Recio, and L. Pueyo, J. Mol. Struct. **426**, 233 (1998).
[10] A.J. Rowley, P. Jemmer, M. Wilson, and P.A. Madden, J. Chem. Phys. **108**, 10 209 (1998).
[11] A. Aguado, L. Bernasconi, and P.A. Madden, J. Chem. Phys. **118**, 5704 (2003); A. Aguado and P.A. Madden, *ibid.* **118**, 5718 (2003).
[12] A. Aguado, L. Bernasconi, and P.A. Madden, Chem. Phys. Lett. **356**, 437 (2002); L. Bernasconi, P.A. Madden, and M. Wilson, Phys. Chem. Comm. **1** (2002); A. Aguado, L. Bernasconi, S. Jahn, and P.A. Madden, Faraday Discuss. **124**, 171 (2003).
[13] H. Cynn, D.G. Isaak, R.E. Cohen, M.F. Nicol, and O.L. Anderson, Am. Mineral. **75**, 439 (1990).
[14] F.C. Marton and R.E. Cohen, Am. Mineral. **79**, 789 (1994).
[15] M.S.T. Bukowinski, A. Chizmeshya, G.H. Wolf, and H. Zhang, Mol. Eng. **6**, 81 (1996).
[16] R.E. Cohen, Geophys. Res. Lett. **14**, 37 (1987).
[17] M. Wilson, J. Am. Ceram. Soc. **81**, 2558 (1998).
[18] W. H. Press, S. A. Teukolsky, W. T. Vetterling, and B. P. Flannery, *Numerical Recipes* (Cambridge University Press, Cambridge, 1992).
[19] S. Nosé and M.L. Klein, Mol. Phys. **50**, 1055 (1983).
[20] G.J. Martyna, D.J. Tobias, and M.L. Klein, J. Chem. Phys. **101**, 4177 (1994).
[21] D. T. Cromer and J. T. Waber, in *International Tables for X-ray Crystallography*, edited by J. A. Ibers and W. C. Hamilton (Kynoch Press, Birmingham, 1974), p. 71.
[22] A.G. Marinopoulos and C. Elsässer, Acta Mater. **48**, 4375 (2000).
[23] T. Vosegaard and H.J. Jakobsen, J. Magn. Reson. (1969-1992) **128**, 135 (1997); A.J. Woo, Bull. Korean Chem. Soc. **20**, 1205 (1999).
[24] C. Elsässer and A.G. Marinopoulos, Acta Mater. **49**, 2951 (2001).